Photochemical & Photobiological Sciences

Accepted Manuscript

This is an *Accepted Manuscript*, which has been through the Royal Society of Chemistry peer review process and has been accepted for publication.

Accepted Manuscripts are published online shortly after acceptance, before technical editing, formatting and proof reading. Using this free service, authors can make their results available to the community, in citable form, before we publish the edited article. We will replace this *Accepted Manuscript* with the edited and formatted *Advance Article* as soon as it is available.

You can find more information about *Accepted Manuscripts* in the Information for Authors.

Please note that technical editing may introduce minor changes to the text and/or graphics, which may alter content. The journal's standard Terms & Conditions and the Ethical guidelines still apply. In no event shall the Royal Society of Chemistry be held responsible for any errors or omissions in this *Accepted Manuscript* or any consequences arising from the use of any information it contains.

ROYAL SOCIETY OF CHEMISTRY

www.rsc.org/pps

Photochemical & Photobiological Sciences

Photochemical & Photobiological Sciences

Dynamic Article Links ►

Cite this: DOI: 10.1039/c0xx00000x

ARTICLE TYPE

www.rsc.org/xxxxxx

Effective Photocatalytic Dechlorination of 2,4-Dichlorophenol by A Novel Graphene Encapsulated ZnO/Co_3O_4 Core-shell Hybrid under Visible Light

Md.Rakibuddin and Rajakumar Ananthakrishnan*

Received (in XXX, XXX) Xth XXXXXXXXX 20XX, Accepted Xth XXXXXXXXX 20XX
DOI: 10.1039/b000000x

In the present work, graphene encapsulated ZnO/Co_3O_4 (GE/ZnO/Co_3O_4) core-shell hybrid is fabricated through a facile self-assembly approach, where the mutual electrostatic interaction force drives the ZnO/Co_3O_4 heteronanostructures to be fully wrapped with flexible ultrathin graphene shells. As-prepared GE/ZnO/Co_3O_4 core-shell hybrid is characterized and exhibits excellent visible light photocatalytic ability toward dechlorination of 2,4-dichlorophenol (2,4-DCP) in aqueous phase. It is worth noting that the 2,4-DCP is almost completely mineralized into CO_2 and H_2O by the GE/ZnO/Co_3O_4 after 5 h of photocatalytic reaction. This type of higher dechlorination and mineralization efficiency of the 2,4-DCP is not generally observed, and is found to be higher than some previous studies. The dechlorination of 2,4-DCP has been achieved under different parametric conditions. The unique architecture of the GE/ZnO/Co_3O_4 core-shell hybrid also provides high stability and recyclability towards degradation of 2,4-DCP. The higher photocatalytic activity of the hybrid can be ascribed by synergistic effect of ZnO, Co_3O_4 and graphene, and also by an increase in contact surface between metal oxides core and graphene shell, which acts as a continuous path for rapid electron transport to offer more number of reactive species.

Introduction

Semiconductor photocatalytic technology, a well-accepted strategy, has attracted tremendous attention because of its potential for hydrogen generation and pollutants degradation to simultaneously solve the energy and environmental crises.[1] In recent years, graphene−inorganic semiconductor composite materials have got widespread concern for the researchers in the area of solar energy conversion.[2,3] Graphene, a zero band gap two-dimensional (2D) sp^2-hybridized carbon atoms with platelike structures possess very high charge carrier mobility, specific surface area, excellent optical properties, transparency, mechanical flexibility as well as good thermal and chemical stability, which makes it an excellent electron-transport material for photocatalysis even more appropriate than C_{60}, polyaniline and graphite-like carbon.[4-6] In particular, due to the large-size 2-D structure, the graphene sheet could behave as a giant solid support (stabilizer) of nanoparticles through interfacial interaction to avoid particle aggregation, and plenty of p electrons present in the special π-conjugation structure of the graphene provide a suitable platform for the growth and stability of inorganic nanoparticles.[7,8] Graphene could enhance the photocatalytic activity of a catalyst by increasing the reaction active sites and facilitating the adsorption of organic contaminants.[9] Furthermore, a strong heterojunction electric field is formed on the interface between graphene and an inorganic semiconductor material due to the difference in their Fermi levels.[10] Photogenerated electrons are swiftly transferred to the graphene surface and participate in the reduction reactions occurring there, which enhances the separation efficiency of photogenerated electron−hole pairs and also the photocatalytic ability significantly.

Metal oxide nanocomposites composed of two or more dissimilar materials with attractive performance are currently in the spotlight to improve diverse properties of functional materials.[11] An interface is created by the partial reaction of two oxides, which shows some novel attractive properties because of the influence of proximity and diffusion phenomena at the nanoscale range.[12,13] Based on this idea, various ZnO-based heterostructures have been designed for various interesting properties.[14-16] ZnO, an n-type semiconductor, is well known for its versatile application,[17] while p-type Co_3O_4 is recognized for high catalytic activity and lithium storage capacity.[18,19] It is

Department of Chemistry, Indian Institute of Technology, Kharagpur 721302, India. E-mail: raja.iitchem@yahoo.com; Fax: +91 3222-282252; Tel: +91 3222-282322

†Electronic supplementary information (ESI) available: Supporting information is available free of charge via internet at hppt://pubs.rsc.org/.

desirable that the synergistic combination of ZnO and Co_3O_4 will display some novel fascinating properties. In recent years, reasonable number of literature reports are available on ZnO/Co_3O_4 exhibiting their potential application in gas sensing and catalytic behaviour.[17,20] Owing to the rise of graphene in recent times, combinations of graphene with semiconductors such as, TiO_2,[21] ZnO,[22] CdS, [23] SnO_2 [24] etc. are becoming popular for various applications. In these materials, the metal oxides are distributed into the graphene surface or between the graphene layers significantly improving the photocatalytic activity. However, it is important to note that the contact area between graphene and the inorganic semiconductor materials is relatively small and the effective area of the heterojunction built on the interface is low, as a result, it cannot display optimum photocatalytic performance.[2] Also the metal oxide nanoparticles still can go strong aggregation because of non-intimate contact between the graphene layers and metal oxides. One of the most promising strategies to tackle the aggregation problem of metal oxides is either to confine them within individual carbon shells or the usage of graphene coated metal oxide surface. For example, Yang et al. synthesized graphene encapsulated Co_3O_4 for high-performance Li ion battery.[25] Bu and co-workers fabricated graphene coated ZnO quasi-core-shell composite for high photocatalytic performance.[10] However, the photocatalytic activity of ZnO/Co_3O_4 hybrid has not been well explored so far. Recently, we have shown higher gas sorption and photocatalytic activity of porous ZnO/Co_3O_4 hybrids obtained from a coordination polymer route.[26] However, to the best of our knowledge, the synergistic effect and enhanced photocatalytic activity towards dechlorination of chlorinated phenols for this new type core-shell hybrid of ZnO/Co_3O_4 and graphene has not been yet explored.

Hence, in this report, ZnO/Co_3O_4 heteronanostructures are first prepared from a facile thermal treatment of a coordination polymer precursor. The as-prepared ZnO/Co_3O_4 is fabricated with graphene to obtain graphene encapsulated ZnO/Co_3O_4 ($GE/ZnO/Co_3O_4$) core-shell type hybrid. The overall synthetic procedure of $GE/ZnO/Co_3O_4$ involves three steps: firstly, the ZnO/Co_3O_4 is modified by surface grafting of aminopropyltriethoxysilane (APTES) to make the surface positively charged[25] (Scheme 1). In second step, the amine-treated ZnO/Co_3O_4 is assembled with negatively charged GO by the mutual electrostatic interactions of the two species. Finally, the resulting aggregates are reduced with hydrazine hydrate to make the $GE/ZnO/Co_3O_4$ core-shell type hybrid, where the graphene surface encapsulates the ZnO/Co_3O_4 core from the outer shell. The as-prepared $GE/ZnO/Co_3O_4$ further exhibits excellent performance towards mineralization of 2,4-DCP under visible light. The enhanced photocatalytic activity of $GE/ZnO/Co_3O_4$ core-shell hybrid can be ascribed by several factors; i) synergistic effects of presence of both metal oxides and graphene improves visible light absorption, ii) formation of a core-shell type hybrid where graphene shells are very close in contact with metal oxides core wrapping all around (contact area increases) and acting as a continuous path for very rapid electron transport, iii) very high surface area of the $GE/ZnO/Co_3O_4$ hybrid and also the porous ZnO/Co_3O_4 adsorb organic molecules along with graphene, hence more number of reactant molecules are bound to the catalyst surface, iv) it suppresses the recombination of electron-holes and hence, prolongs the lifetimes of the carriers resulting more hydroxyl and superoxide radicals, and v) the unique core-shell architecture prevents aggregation and photo-corrosion of ZnO/Co_3O_4 core more effectively and makes it high stable towards degradation of 2,4-DCP.

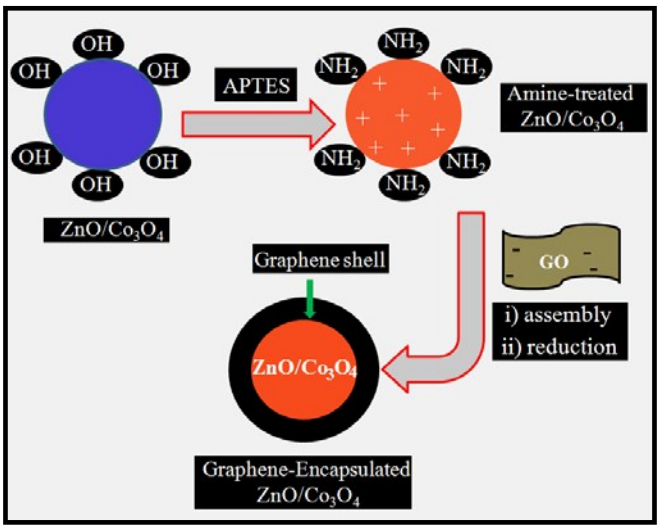

Scheme 1. Schematic representation of the formation of the $GE/ZnO/Co_3O_4$ core-shell hybrid from ZnO/Co_3O_4 prepared from a nano coordination polymer route.

Experimental

Reagents and materials

The 2,3-dihydroxybenzaldehyde and Zinc acetate dihydrate were obtained from Sigma-Aldrich and SISCO Research Laboratories Pvt. Ltd. (India), respectively and used as received. Cobalt acetate tetrahydrate was obtained from Loba Chemie Pvt. Ltd (India). 3-aminopropyltriethoxy silane (APTES) was purchased from Spectrochem Pvt. Ltd. (India). All other chemicals (solvents) used in this investigation were analytical grade (99.9%). All the solutions were prepared in Millipore water (Milli-Q system).

Preparation of the ZnO-Co_3O_4 heteronanostructures from nano coordination polymers

The ZnO-Co_3O_4 heteronanostructures were prepared according to our previous reported method[26] with slight modifications using 2,3-dihydroxylated salophen ligand (2,3-DHS) and terephthalic acid (1,4-H_2BDC) as linkers with $Zn(OAc)_2{\cdot}2H_2O$ and $Co(OAc)_2{\cdot}4H_2O$ in DMF. In a typical method, 2,3-DHS (0.007 mmol) was dissolved in a minimum amount of DMF. Another DMF solution of $Zn(OAc)_2{\cdot}2H_2O$ (0.021 mmol) and $Co(OAc)_2{\cdot}4H_2O$ (0.028 mmol) was added successively to the above prepared solution. Finally, 5 mL DMF solution of 1,4-H_2BDC (0.035 mmol) was added to the finally prepared solution. Within second hexagonal lump shape NCP was formed. The Zn-Co NCPs obtained were centrifuged and washed with acetonitrile several times and then dried at open air (yield ~70%) for several hours. The produced Zn-Co NCPs were then placed in a conventional furnace and heated at 550 °C for 75 min; finally

hexagonal shaped ZnO/Co_3O_4 nanostructures were generated (Figure S1-2).

Preparation of GO

The graphene oxide was synthesized from natural graphite by modified Hummers method.[27] In a typical method, 1 g of graphite and 0.5 g of sodium nitrate ($NaNO_3$) were mixed with 35 mL of concentrated sulphuric acid. After that, the mixture was stirred for 30 min in an ice bath, and 3.6 g of potassium permanganate ($KMnO_4$) was added under vigorous stirring. The rate of addition was carefully controlled to keep the reaction temperature lower than 20 °C. The mixture was then continuously stirred at room temperature for overnight, and 150 mL of deionized (DI) water was slowly added under vigorous agitation. The obtained diluted suspension was stirred for one day, and 10 mL of 30 wt% H_2O_2 was added to the mixture. Finally, the mixture was washed by rinsing and centrifuging with 5 wt% HCl and DI water for several times. Chemical exfoliation of thus-obtained graphite oxide was carried out in an ultrasonic bath for 90 min to obtain GO.

Preparation of the GE/ZnO/Co_3O_4 core shell hybrids

The GE/ZnO/Co_3O_4 core-shell hybrids were obtained via electrostatic interaction between APTES modified oxides and graphene oxide in aqueous solutions. Firstly, the ZnO/Co_3O_4 was modified with APTES to introduce a positively charged surface. In a typical process, ZnO/Co_3O_4 (0.5 g) was dispersed into 50 mL of isopropanol via ultrasonication. Then, 0.5 mL APS was added into the above solution and refluxed at 80 ^{0}C for 24 h. After washing with ethanol several times, the APTES modified ZnO/Co_3O_4 (APTES/ZnO/Co_3O_4) was obtained. Next, the dried APTES/ZnO/Co_3O_4 was dispersed in 100 mL ultrapure water followed by the addition of 150 mL aqueous GO suspension (0.5 mg/mL) and the overall pH of the solution was measured to be 6.0. At this pH, the modified ZnO/Co_3O_4 was assembled with negatively charged GO by electrostatic interactions. After mildly stirring for 30 min, 10 mL of hydrazine hydrate solution (35 wt%) was added into the above aggregates to reduce the GO, and finally the GE/ZnO/Co_3O_4 was obtained after centrifugation and washing with ultrapure water.

The surface charges of APTES/ZnO/Co_3O_4 and GO were examined at different pH solutions by zeta potential measurements. As shown in Figure S3, the surface of GO was negatively charged (zeta potential= –23–53 mV) over the investigated pH range (2–11) due to ionization of the carboxylic acid and phenolic hydroxyl groups located on the GO.[21] The surface charge of the APTES/ZnO/Co_3O_4 switched from positive (zeta potential= +50 mV) to negative (zeta potential= –45 mV) with an increase of the pH value from 2 to 11. It indicates that the mutual assembly can only be triggered when APTES/ZnO/Co_3O_4 and GO were oppositely charged, hence suggesting that the electrostatic interaction was the driving force.

Visible light photocatalytic experiments

The photocatalytic activity of the as-synthesized GE/ZnO/Co_3O_4 core-shell hybrid was measured in 30 mL of reaction mixture of 2,4-DCP (20 mg/L) in an aqueous medium. 1 g/L of the hybrid catalyst was taken in a Pyrex glass vessel and stirred in the dark for 30 min to maintain adsorption equilibrium between the pollutant and the surface of the catalyst under room air-equilibrated conditions. Then, the final mixture was irradiated by 300 W Phillips visible lamps containing aqueous $NaNO_2$ solution (10% w/w) as a UV-cut off filter. After a certain regular interval of time, exactly 5 mL of an aliquot was taken from the reaction mixture and centrifuged to separate the catalyst. Thus, the obtained clear solution was preserved for spectral analysis.

GC-MS study

The photocatalytic degradations of 2,4-DCP were repeated several times under optimized conditions. After 2 h and 5 h of the photoreaction, the reaction mixtures (after centrifuged) were collected separately. Then, the obtained mixture were extracted firstly with chloroform, dichloromethane and ethyl acetate, and finally with diethyl ether. All the organic solvents were collected and removed under reduced pressure using rotary evaporator. Finally, the products obtained were dried under vacuum and dissolved in HPLC grade methanol for GC-MS analysis.

Results and Discussion

Characterization of the synthesized GE/ZnO/Co_3O_4 core-shell hybrid

To determine the phase composition and surface functional in GE/ZnO/Co_3O_4 core/shell heterostructures FT-IR studies are carried out. Figure 1 shows FTIR spectra of graphite, GO, bare $ZnO-Co_3O_4$, and GE/ZnO/Co_3O_4. It is noted that no significant peak is found for the graphite, while the presence of different type of oxygen functionalities in graphene oxide are confirmed by O-H stretching vibrations at 3400 cm^{-1}, O–H deformation vibrations at 1415 cm^{-1}, C=O stretching vibrations at 1720 cm^{-1}, carboxyl C-OH stretching vibrations at 1216 cm^{-1} and alkoxy C-O-C stretching at 1055 cm^{-1}. Besides, the aromatic C=C skeletal vibration of the sp^2 domains (1565 cm^{-1}) is also present in the GO.

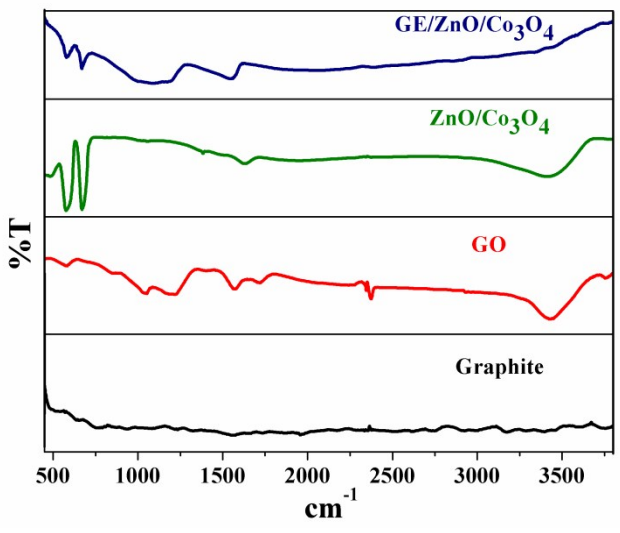

Figure 1. FT-IR spectra of the Graphite, GO, ZnO/Co_3O_4 and GE/ZnO/Co_3O_4 hybrid.

Compared with the IR spectrum of GO, it is observed that the oxygen-containing functional peaks decrease to a large extent and even disappeared for the GE/ZnO/Co_3O_4 hybrid, further indicating that the GO is reduced to graphene after the solvothermal reaction. In addition, the skeletal vibration of the

graphene sheets[28] is emerged at 1545 cm^{-1} for the GE/ZnO/Co_3O_4 hybrid. In the IR spectra of the GE/ZnO/Co_3O_4 hybrid, absorption bands at 482 cm^{-1}, 572 and 677 cm^{-1} are attributed to the vibration of Zn–O, Co^{3+}-O and Co^{2+}-O bonds[25], respectively, indicating the existence of ZnO and Co_3O_4 in the hybrid. Also, three new absorption bands at 1005 cm^{-1}, 1085 cm^{-1} and 1185 cm^{-1} originating from Si-O-Zn, $(Si-O)_n$ and Si-O-Co bond vibration, respectively[25] are due to grafting of APTES moieties successfully onto the surface of ZnO-Co_3O_4.

Information regarding the phase composition, purity, and crystallinity of the as-synthesized samples is procured by Powder X-ray diffraction (PXRD) analysis, and the results are shown in Figure 2. The XRD peak of natural graphite powder is found at 26.71º exhibiting an interlayer distance of 3.2 A˚. In comparison to the natural graphite, a wide peak at 2θ = 10.27º is observed corresponding to the (001) diffraction of GO, which indicates that the graphite is fully oxidized into GO with an interlayer distance of 8.60 A˚. GO has a larger interlayer distance than graphite since H_2O molecules and various oxide groups intercalate between its layers.[29] From the XRD pattern of the GE/ZnO/Co_3O_4 core-shell hybrid, it is observed that the intensive peaks at 2θ values of 31.7, 34.4, 36.2, 47.5, 56.5, 62.8, 68.0 can be respectively indexed to (100), (002), (101), (102), (110), (103) and (112) diffractions of hexagonal wurtzite phase of the ZnO, which is indexed by an asterisk mark in the figure. Again, the measured peaks observed at 2θ = 31.13, 36.76, 38.5, 44.8, 55.5, 59.2, 65.26 and 77.4 correspond to (111), (220), (311), (222), (400), (422), (511), (440) and (533) planes of cubic phase of Co_3O_4 crystals, respectively (JCPDS, 42-1467).[30] No peaks of impurities are observed in the XRD pattern indicating the formation of single-phase ZnO/Co_3O_4 heteronanostructure. Comparing with pure ZnO/Co_3O_4, an additional characteristic peak around 2θ = 22.27º is found in the XRD pattern, which corresponds to (002) diffraction of the graphene in the GE/ZnO/Co_3O_4 core-shell hybrid demonstrating that GO is fully reduced to graphene by hydrazine upon thermal treatment. The interlayer distance of graphene is found to be 3.5 A˚, which is reduced from the interlayer distance of 8.60 A˚ of GO indicating successful removal of oxygenated functional groups.

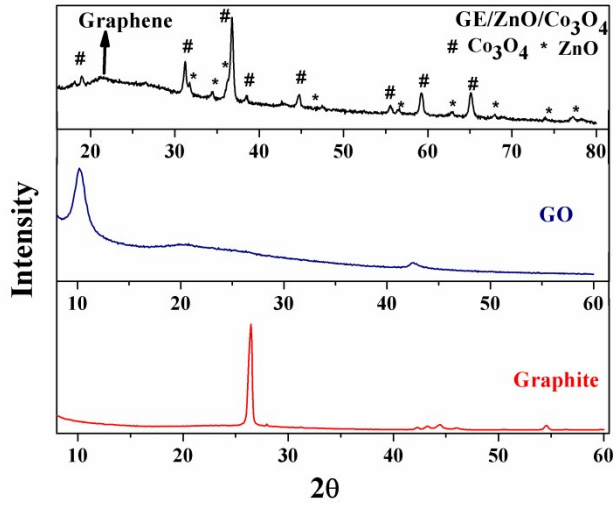

Figure 2. Powder X-ray diffraction pattern of the Graphite, synthesized GO and GE/ZnO/Co_3O_4 hybrid.

X-ray photoelectron spectra (XPS), usually are used to analyze the element component and valence for the materials, and also give information about the interfacial interactions between the components. Figure 3 shows the XPS spectra of the GE/ZnO/Co_3O_4 core-shell hybrid. From the full survey spectrum, the peaks belonging to C, Zn, O, Co, Si and N elements can be observed (Figure 3a). For detailed information, the high-resolution XPS spectra of the C, Zn, Co and O elements are also provided. It is clearly seen (Figure 3b) that the XPS spectrum of C1s can be deconvoluted into three peaks centred at 282.7, 284.6 and 286.5 eV. The peak at 284.6 eV is attributed to the sp^2 carbon atom, while the peak positioned at 286.5 eV is assigned to the C-O groups. The peak located at 282.7 eV is closely associated with the C (sp^3)–Si bond of the APTES.[31] The C species belonging to the sp^2 carbon atom have a high percentage than the other carbon species, and the intensities of all the related oxygen peaks are sharply decreased in the GE/ZnO/Co_3O_4 sample compared to GO indicating that the GE/ZnO/Co_3O_4 contains far less oxygen and delocalized p conjugation is restored in the GE/ZnO/Co_3O_4, hence confirming its high quality. The XPS survey also showed a pronounced peak for N 1s of C-N bond at 399.5 eV[32], which is due to the presence of amine functionalization of APS. Also the Si-O-C bond of APS appears at 101.2 eV[32] in the XPS survey of the GE/ZnO/Co_3O_4 hybrid. Besides the C1s peak, as shown in Figure 3d, the peaks of Zn $2p_{3/2}$ and Zn $2p_{1/2}$ are located at 1021.4 and 1044.4 eV in the GE/ZnO/Co_3O_4 hybrid. The high resolution XPS fitting of Co 2p shows prominent peaks around at 779.3 eV and 794.4 eV, which are attributed to Co^{3+} $2p_{3/2}$ and Co^{3+} $2p_{1/2}$ configuration of the Co_3O_4, respectively, and the fitting peaks at 780.7, 789.1 and 796.4 eV are due to Co^{2+} of the Co_3O_4[33] in the GE/ZnO/ Co_3O_4 core-shell hybrid.

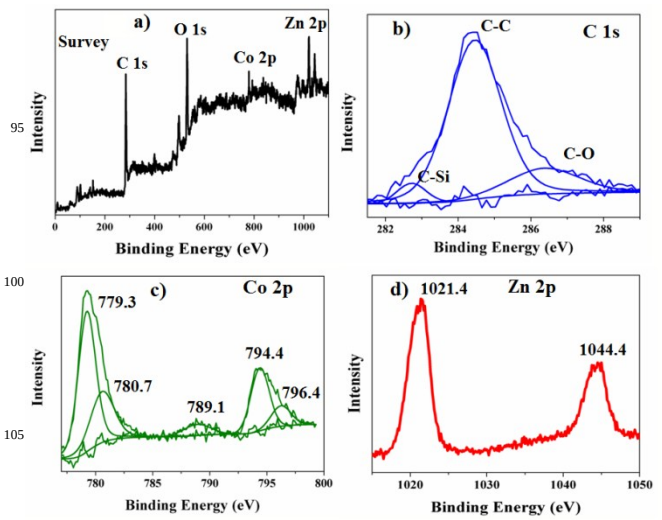

Figure 3. a) XPS full survey of the synthesized GE/ZnO/Co_3O_4 core-shell hybrid, b) High resolution XPS measurement of the C 1s, c) Co 2p and d) Zn 2p of the GE/ZnO/Co_3O_4 core-shell hybrid.

Convincing proof of the core/shell formation in GE/ZnO/Co_3O_4 heterostructures is revealed by TEM and HRTEM studies (Figure 4). In Figure 4a, the TEM image shows the presence of bare GO sheets with uniform distribution. However, after hybrid formation of GO with ZnO/Co_3O_4 and followed by reduction of GO, the TEM images shows (Figure 4b-d) that in most cases thin

graphene shells are wrapped around the surface of ZnO/Co_3O_4 particles. The diameters of the ZnO and Co_3O_4 in the $GE/ZnO/Co_3O_4$ heterostructure are found to be around 40 and 20 nm, respectively. Due to the presence of flexible and ultrathin graphene, the $GE/ZnO/Co_3O_4$ exhibit crinkled and rough textures. The TEM images clearly show that the ZnO/Co_3O_4 particles are firmly attached or interconnected to each other by thin graphene shells via the electrostatic interaction (also see, Figure S4). As shown in Figure 5a-b, the HRTEM image of the $GE/ZnO/Co_3O_4$ core-shell hybrid clearly exhibits the interface of the ZnO or Co_3O_4 core and thin graphene shell.

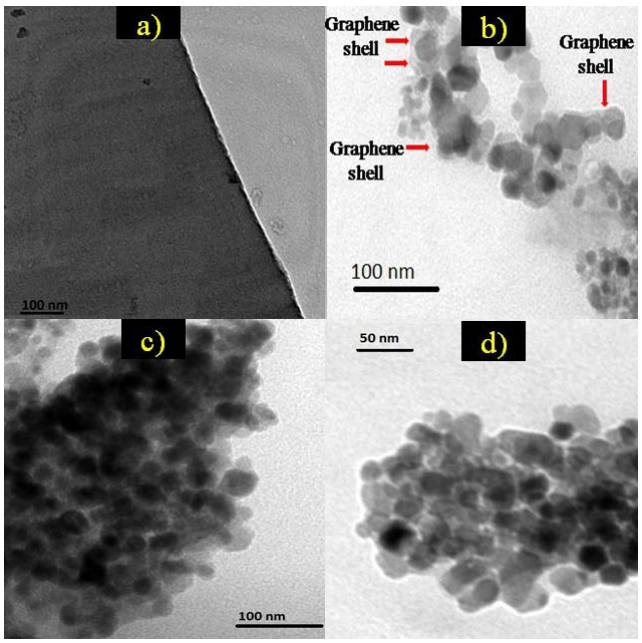

Figure 4. a) TEM image of the prepared GO, and b-c-d) TEM images of the $GE/ZnO/Co_3O_4$ core-shell hybrid.

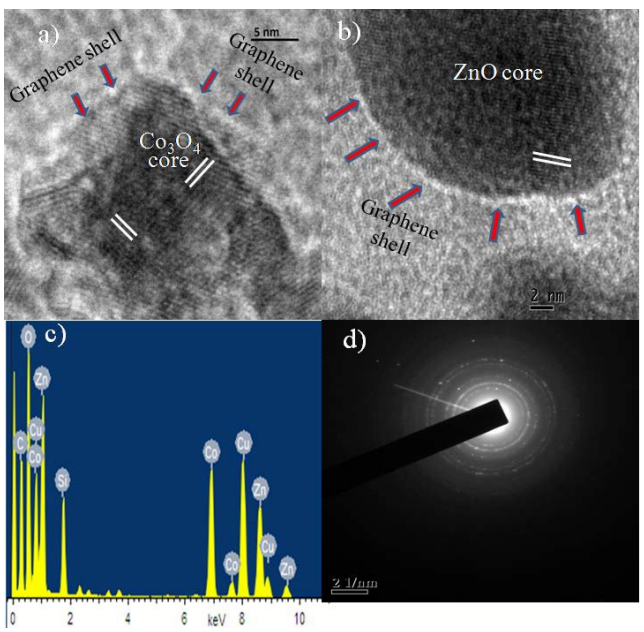

Figure 5. HR-TEM images of the synthesized $GE/ZnO/Co_3O_4$ hybrid showing graphene shell with a) Co_3O_4 core and b) ZnO core and lattice fringes; c) EDX analysis of the $GE/ZnO/Co_3O_4$ hybrid and d) SAED pattern of the $GE/ZnO/Co_3O_4$.

The HRTEM images clearly exhibit lattice fringes with interplanar distance of 0.286 nm and 0.28 nm, which corresponds to the (220) plane of the cubic Co_3O_4 and (100) plane of the hexagonal wurtzite ZnO[34] and thin graphene shells are wrapped around the metal oxides core. The SAED pattern (Figure 5d) indicates polycrystalline nature of the $GE/ZnO/Co_3O_4$ hybrid. The Energy Dispersive X-ray spectroscopy (EDS) displays intense signals of C, Zn, Co and O (Figure 5c) on positioning the electron probe through the core-shell of the $GE/ZnO/Co_3O_4$. The copper and silicon signals come from the Cu grid used for TEM and APTES moiety, respectively. Thus, the TEM and HRTEM analysis confirms the core/shell morphology of $GE/ZnO/Co_3O_4$ hybrids.

TGA analysis and BET surface area of the synthesized $GE/ZnO/Co_3O_4$ hybrid

The quality of as-prepared $GE/ZnO/Co_3O_4$ hybrid is assessed by thermogravimetric analysis (TGA). The samples are heated from room temperature to 600 °C at 5 °C/min under N_2 atmosphere using Al_2O_3 crucible and the results are shown in Figure 6a. The bare ZnO/Co_3O_4 sample shows high thermal stability up to 600 °C without any loss of weight. In contrast, the $GE/ZnO/Co_3O_4$ hybrid exhibits relatively lower thermal stability than bare ZnO/Co_3O_4 due to the presence of grapheme shell.

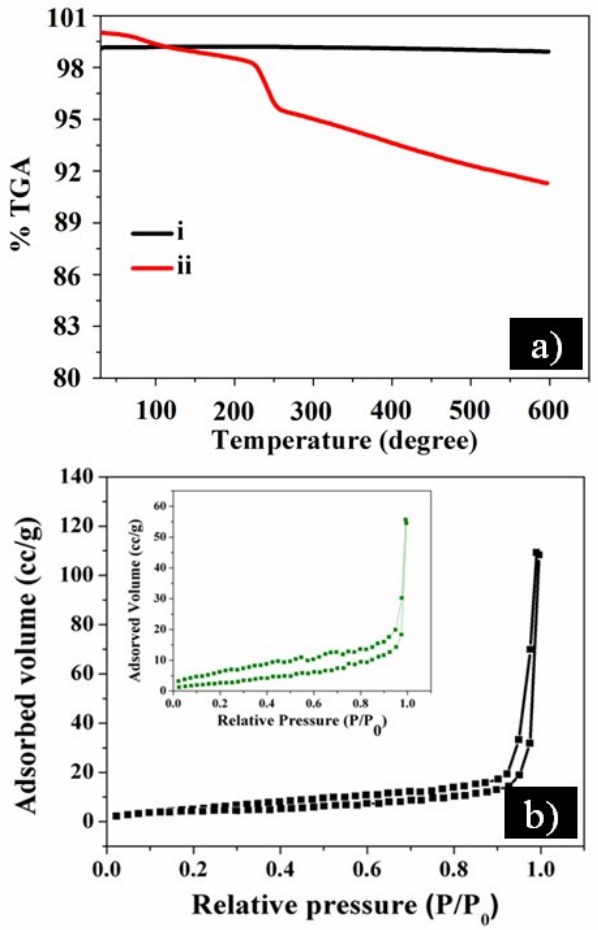

Figure 6. a) TGA curve of the synthesized i) bare ZnO/Co_3O_4 and ii) $GE/ZnO/Co_3O_4$ hybrid; b) BET-N_2 gas sorption isotherm curves of the synthesized $GE/ZnO/Co_3O_4$ and bare ZnO/Co_3O_4 (inset).

The total weight loss for the GE/ZnO/Co_3O_4 is only 9% at 600 °C indicating incorporation of very low weight fraction of graphene shell into the core-shell hybrid. Hence, the weight fraction of ZnO/Co_3O_4 in the core-shell hybrid is as high as 91%, which is much higher than those of reported core–shell metal oxide/carbon composites (40–75%).[35-37] The minor weight loss occurred between 100 and 225 °C indicating the release of CO, CO_2 and stream from the most labile functional groups during pyrolysis.[38] The minor mass-loss is attributed to the absence of most oxygen functional groups of the GO after thermal reduction.

Moreover, the porosity and surface area of the synthesized GE/ZnO/Co_3O_4 core-shell hybrid are characterized by Brunauer–Emmett–Teller (BET) nitrogen adsorption–desorption isotherm measurements. As shown in Figure 6b, the BET isotherms of the prepared hybrid follow type III behaviour, which is a weak van der Waals force of attraction between the adsorbate (N_2 gas) and adsorbents (hybrid). Thus, the isotherms are reversible in nature as soon as the pressure is released. All the curves explain the multilayer sorption property of the materials.[39] It is noted that the BET specific surface area (250.2 m^2/g) and pore volume (0.435 cc/g) of GE/ZnO/Co_3O_4 core-shell hybrid are significantly higher than that of the bare ZnO/Co_3O_4 (100.4 m^2 g^{-1} and 0.223 cc/g, respectively).

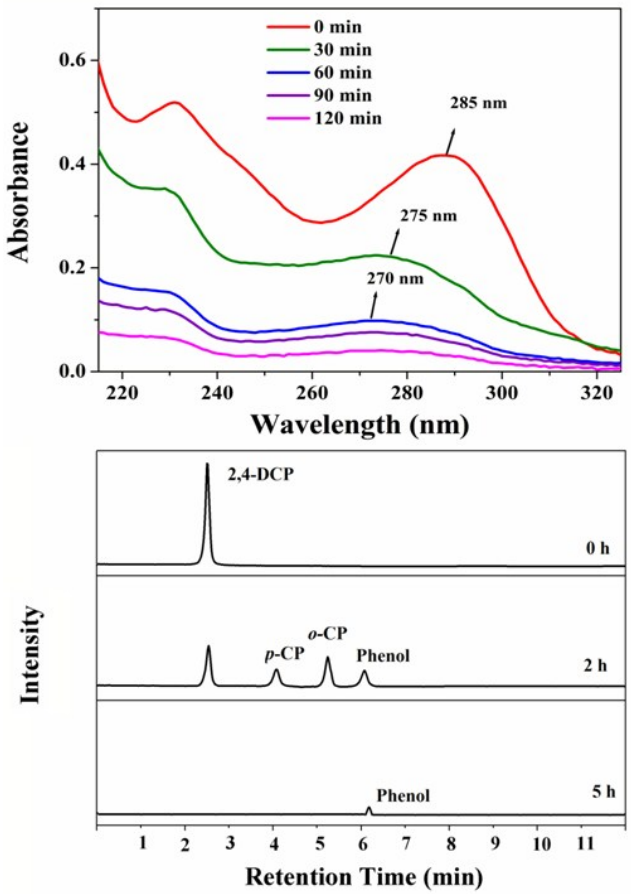

Figure 7. a) UV- Visible absorption spectra of the 2,4-DCP degradation in presence of the GE/ZnO/Co_3O_4 hybrid ([2,4-DCP]=20 mg/L , [catalyst]= 1.0 g/L, pH=5.0), and b) HPLC analysis of total ion chromatogram for the degradation of 2,4-DCP under different interval of time: 0 h, 2 h and 5 h.

The high specific surface area and porosity of the GE/ZnO/Co_3O_4 could be attributed to the presence of wrapped graphene shell as well as the formation of secondary pores between the porous ZnO/Co_3O_4 and the graphene. Hence, the high surface area and porosity of GE/ZnO/Co_3O_4 hybrid could promote higher photocatalytic activity by adsorbing more number of organic reactant molecules on the catalyst surface.

Visible light photocatalytic degradation of 2,4-DCP

Chlorophenol compounds are a major class of environmental pollutants and potential human carcinogens.[40] This class of compounds can easily be accumulated in biological tissues, which poses a great threat to agriculture, food chain and human health.[41] 2,4-DCP, a highly toxic and an important reagent in the manufacture of pesticides and herbicides[42] has been identified as a primary pollutant by United States Environmental Protection Agency (USEPA). Therefore, it is highly desirable to develop efficient methods or catalyst for the removal of 2,4-DCP from water bodies transforming this class of compounds into non-toxic product or CO_2 and H_2O. Consequently, the removal of 2,4-DCP is relevant in this current report. Recently, visible light assisted photocatalytic degradation of various organic pollutants and synthesis of some important organic molecules has been reported by our group.[43-47]

The photocatalytic activities of the GE/ZnO/Co_3O_4 core-shell hybrids are evaluated by taking 30 mL of reaction mixture of 2,4-DCP (20 mg/L) in aqueous medium and catalytic amount (1 g/L) of the hybrids, and before irradiation, it is kept in the dark under magnetic stirring for 30 min to maintain adsorption/desorption equilibrium between the pollutant and the surface of the catalyst. The adsorption of 2,4-DCP on the catalysts could be attributed to the adsorption of 2,4-DCP on the RGO shell and on the core of the porous metal oxide nanostructure. The former seemed to be much more favourable because of its giant p-conjugational plane, which strongly interacts with DCP molecules via a p–p stacking with a face-to-face orientation. The photodegradation of 2,4-DCP is monitored using both HPLC and UV-Visible absorption spectrophotometer by measuring the concentration of 2,4-DCP at different time intervals.

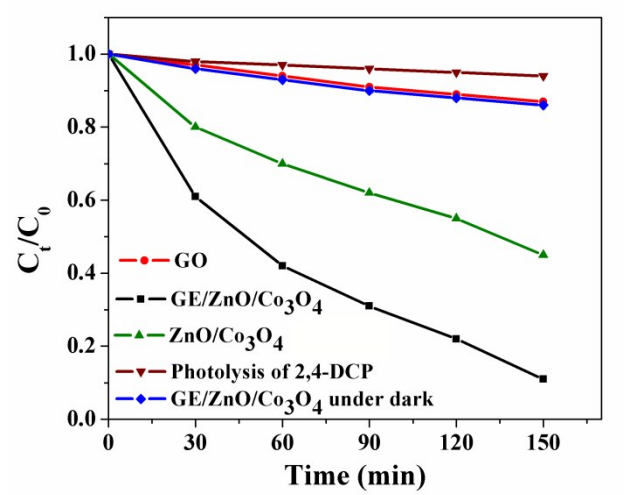

Figure 8. Kinetic plots (C_t/C_0 *vs* Time) for the visible light ($\lambda \geq 420$ nm) photocatalytic degradation of 2,4-DCP in the presence of GE/ZnO/Co_3O_4 hybrid with control studies.

The UV-Visible absorption spectra of the 2,4-DCP degradation is shown in Figure 7a. The 2,4-DCP exhibits its maximum absorption at 285 nm, hence decrease in intensity of the peak 285 nm are used to measure the concentration of 2,4-DCP. After 30 min, the peak at 285 nm is blue-shifted to 275 nm due to dechlorination of 2,4-DCP to *o*-chlorophenol (*o*-CP), which is further decomposed to phenol identified by the peak at 270 nm in UV spectra after 60 min.[48] Finally, the phenol is mineralized into CO_2 and water. This information has been also supported by total ion chromatogram of the reaction products of 2,4-DCP carried out by HPLC (Figure 7b). The 2,4-DCP was decomposed into *o*-CP, *p*-CP and phenol after 120 min of photocatalytic reaction. The concentration of 2,4-DCP is sufficiently decreased, and the peak intensity demonstrates that the generation of *o*-CP is more than that of *p*-CP. However, after carrying out the reaction up to 5 h, the products *o*-CP, *p*-CP and 2,4-DCP are vanished and very small amount of phenol is observed indicating maximum mineralization of the above products. The products *o*-CP, *p*-CP and phenol are identified by the retention time of the standard samples under identical conditions and same concentrations (Figure S5).

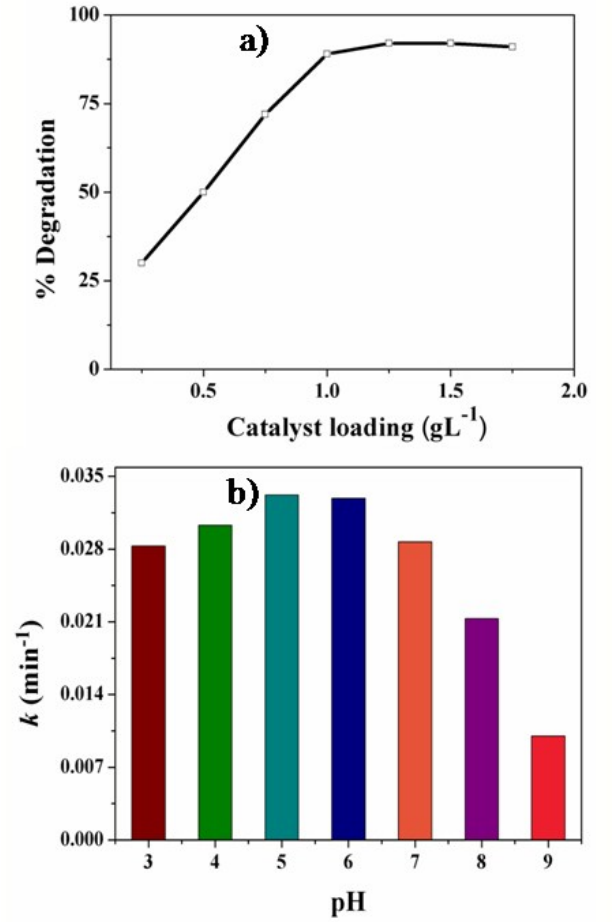

Figure 9. Effect of a) catalyst loading and b) pH of solution for the dechlorination of 2,4-DCP. Experimental conditions: [GE/ZnO/Co_3O_4]= 0.25-1.75 g/L, pH= 3-9, [2,4-DCP]=20 mg/L.

To measure mineralization efficiency of the GE/ZnO/Co_3O_4 catalyst, TOC is analysed after different time intervals. The results show that up to 2 h, TOC removal efficiency is only 35% and this can be attributed to the higher rate of conversion of 2,4-DCP to the *o*-CP, *p*-CP and phenol during the first 2 h. And, the TOC removal finally reached to 93% after 5 h of reaction (Figure S6). However, complete mineralization (100%) of the 2,4-DCP has not been achieved by the GE/ZnO/Co_3O_4 catalyst, as very small percentage of phenol is leaved as the final product indicated by HPLC. However, the high TOC removal value indicates its excellent efficiency toward degradation of 2,4-DCP converting to CO_2 and H_2O, and the value is found to be higher than other reported literatures. [49-51]

It can be seen from Figure 8 that the 2,4-DCP is very stable under visible light irradiation without presence of any photocatalyst. It is slightly degraded (~10%) in the presence of GO. However, in presence of the catalysts GE/ZnO/Co_3O_4, the degradation of 2,4-DCP is remarkably enhanced (91% degraded only after 150 min) with rate constants of about 3.38×10^{-2} min^{-1} (Figure S7) under visible irradiation. The visible light photo-degradation rate of 2,4-DCP in presence of the GE/ZnO/Co_3O_4 catalyst is much faster than other reported literatures.[50,52] However, the photocatalytic activity is significantly decreased (2 times lower) with rate constant of about 1.7×10^{-2} min^{-1} when bare ZnO/Co_3O_4 is applied as a catalyst. Interestingly, when the photodegradation of 2,4-DCP in presence of the GE/ZnO/Co_3O_4 hybrids is carried out under dark condition, no significant degradation is observed (~12%). This results infers that visible light is an essential component for degradation of the 2,4-DCP.

Optimization of reaction conditions

Effect of catalyst dose

The photodegradation of 2,4-DCP is carried out at various catalyst dosages from 0.2 to 2.0 g/L to optimize the reaction conditions. The Figure 9a shows that the photodegradation efficiency is increased with increase in catalyst loading up to 1.25 g/L and then reaches a plateau. Further increase in catalyst dosage did not increase the degradation efficiency. This enhancement at low catalyst loading can be attributed to the increased number of available active sites for 2,4-DCP adsorption and light absorption, which leads to higher number of hydroxyl and/or superoxide radicals.[53] Beyond the optimum point (1.25 g/L), the adverse effect of higher catalyst dosage on the degradation rate is observed. In fact, particle agglomeration at higher concentration limits the light penetration as well as 2,4-DCP adsorption on the available surface of the catalyst. Furthermore, with high catalyst dosages, increased turbidity of the suspension and also light scattering by the particles prevent efficient light-harvesting,[54] which result in a decrease in illuminated active sites on the catalyst surface.[55]

Effect of pH of the solution

In heterogeneous photocatalysis, surface property of semiconductors plays a significant role as reaction takes place on the surface of photocatalyst. Therefore, acid-base condition of the metal oxide surfaces can have a large impact on the adsorption-desorption and photocatalytic degradation performance.[54] The influence of pH on the photodegradation of 2,4-DCP is examined between pH 3.0 to 9.0, as shown in Figure 9b. The rate of 2,4-DCP degradation is very fast between pH 3 to 6, but further increase in pH the degradation rate is declined slightly at pH 7, and significantly beyond pH 8.0 to 9.0. Hence, the degradation of

2,4-DCP is favoured at slightly acidic conditions. This can be explained based on the point of zero charge pH (pH_{pzc}) of the semiconductors. The pH_{pzc} for Co_3O_4 and ZnO are found to be 7.3 and 9.0, respectively from zeta potential analysis.[56,57] Therefore, both the Co_3O_4 and ZnO surfaces are positively charged in acidic condition (pH < 7.3), whereas they are negatively charged under alkaline condition (pH > 9.0). Hence, in slightly acidic to neutral condition, more 2,4-DCP molecules are adsorbed on positively charged surface of the catalyst, thereby enhancing the degradation rate. In contrast, in alkaline condition, less surface interaction is possible between the negatively charged surfaces and negatively charged phenolic molecules, impeding the adsorption on the catalyst surface, hence degradation rate drastically decreases. However, it is important to note that at pH 8, Co_3O_4 surface is negatively charged and ZnO is positively charge, and these two effects oppose each other, hence the photodegradation rate of 2,4-DCP remains at intermediate stage.

Stability of the GE/ZnO/Co_3O_4 hybrid in multiple runs

To check photostability of the GE/ZnO/Co_3O_4 core-shell hybrid, the photodegradation of 2,4-DCP is repeated up to seven cycles under the same conditions, and a set of five cycles is provided in the discussion. The repeatability cycles are performed after washing with ethanol and water several times to remove any unreacted adsorbed DCP molecules from the surface of the core-shell hybrid catalyst to bring the material to its original condition. The GE/ZnO/Co_3O_4 catalyst maintained high photocatalytic activity and does not show any noticeable decline after five successive cyclic operations to degrade 2,4-DCP (Figure 10). It is worth noting that the GE/ZnO/Co_3O_4 catalyst possess much higher photostability and activity than other graphene based ternary composites where this type of core-shell hybrid has not been applied.[58-60] It is quite interesting to see that the bare ZnO/Co_3O_4 in the absence of the graphene shell significantly loses its catalytic efficiency after each successive cycle. This is due to the photoleaching and photocorrosion, which is normally observed for the metal oxides heteronanostructures.

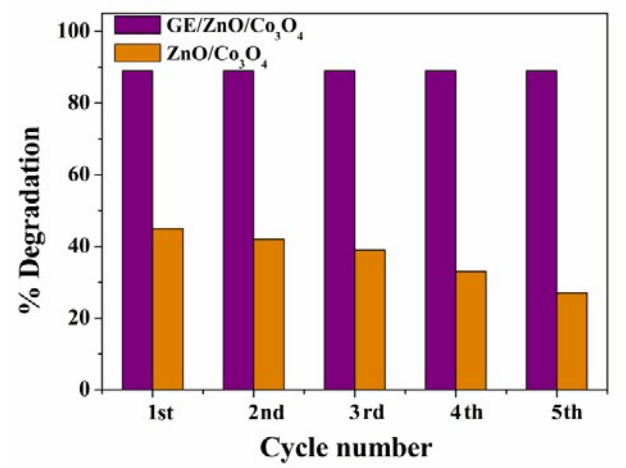

Figure 10. Reusability of the GE/ZnO/Co_3O_4 and ZnO/Co_3O_4 hybrid for the 2,4-DCP degradation.

Nevertheless, introduction of thin graphene shell protects significantly the ZnO/Co_3O_4 core hybrid from photocorrosion or photodissolution and ion leaching, and therefore, providing the catalyst excellent long-term stability and good catalytic performance, and hence offers great promise for environmental purification of aromatic compounds. The catalyst samples before and after photodegradation of 2,4-DCP are also investigated by PXRD and TEM study. The PXRD patterns (Figure S8a) indicate that there is no remarkable alteration or shift of the peak in the crystal structure of the catalyst after 5th cycle of operation. However, there is only 1% loss of photoactivity after 5th cycles, which may be due to some loss of samples during washing. The TEM image of the hybrid after 5th cycle shows (Figure S8b) the ZnO/Co_3O_4 core still is wrapped by graphene shells and hence no noticeable change in morphology is observed for the hybrids.

Scavenger study and photocatalytic mechanism of the GE/ZnO/Co_3O_4 core-shell hybrid

To gain more in-depth knowledge about the photocatalytic mechanism, benzoquinone[61] (BQ), dimethylsulfoxide[62] (DMSO) and ammonium oxalate[63] has been used as scavenging species in order to investigate the generation and roles of $O_2^{\cdot-}$, $OH^{\cdot}$ and (h^+), respectively. The scavengers (10^{-3} M) are introduced prior to the addition of the catalyst to the solution of 2,4-DCP. The Figure 11 shows that the degradation of 2,4-DCP is inhibited in presence of these scavengers with the following order BQ (3.6×10^{-3} min^{-1})> DMSO (1.7×10^{-2} min^{-1}) > formate (2.4×10^{-2} min^{-1}).

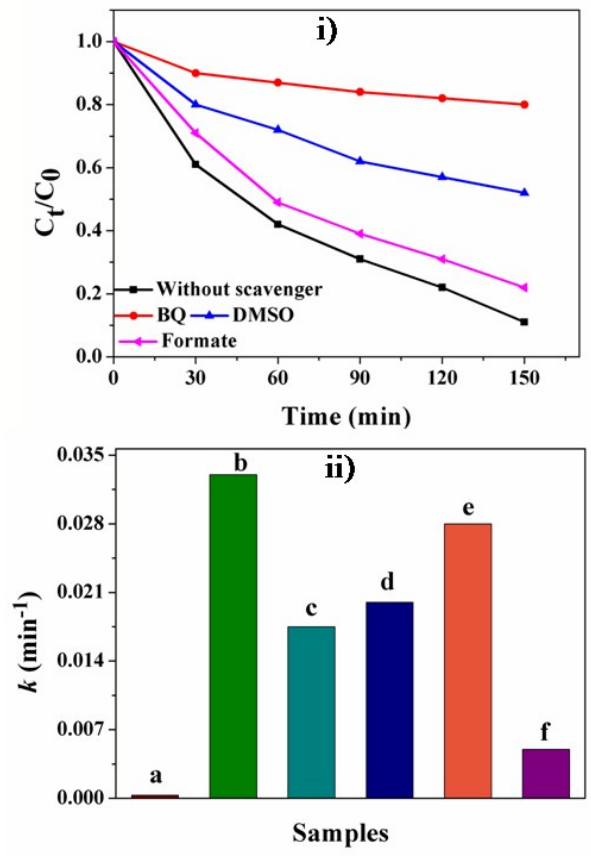

Figure 11. i) Kinetics plots (C_t/C_0 vs time) of the photodegradation of 2,4-DCP under different scavengers; ii) The kinetic constants for the photocatalytic degradation of 2,4-DCP under visible light irradiation in presence of a) GO, b) GE/ZnO/Co_3O_4 , c) GE/ZnO/Co_3O_4 + DMSO, d) bare ZnO/Co_3O_4, e) GE/ZnO/Co_3O_4 + formate and f) GE/ZnO/Co_3O_4 + BQ ([catalyst]= 1.0 g/L, pH= 5.0, [2,4-DCP]=20 mg/L).

The GE/ZnO/Co_3O_4 exhibits only 15% and 30% degradation efficiency of 2,4-DCP in 150 min under visible light after introducing BQ and DMSO into the system, respectively. However, in presence of ammonium oxalate, the degradation of 2,4-DCP is not decreased significantly indicating that holes are not main active species formed in the reaction. Thus, it is postulated that $O_2^{\cdot-}$ followed by $OH^{\cdot}$ are the primarily active intermediates substantially contributed to the degradation of 2,4-DCP, while the role of h^+ is less significant. The catalytic process of the GE/ZnO/Co_3O_4 is further confirmed by the detection of $OH^{\cdot}$ by a photoluminescence (PL) technique using terephthalic acid (TA) as a probe molecule.[63] Figure 12 shows the changes of PL spectra of TA solution with the catalyst under visible light irradiation with irradiation time.

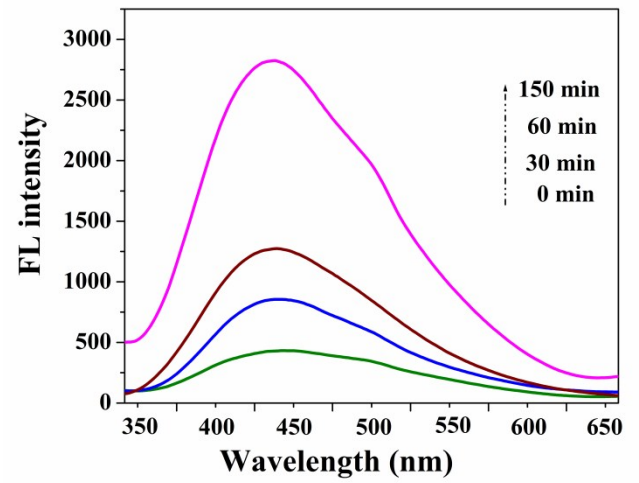

Figure 12. PL spectra changed with visible light irradiation time on GE/ZnO/Co_3O_4 hybrid in a 5 × 10^{-4} mol/L basic solution of TA (excitation at 325 nm).

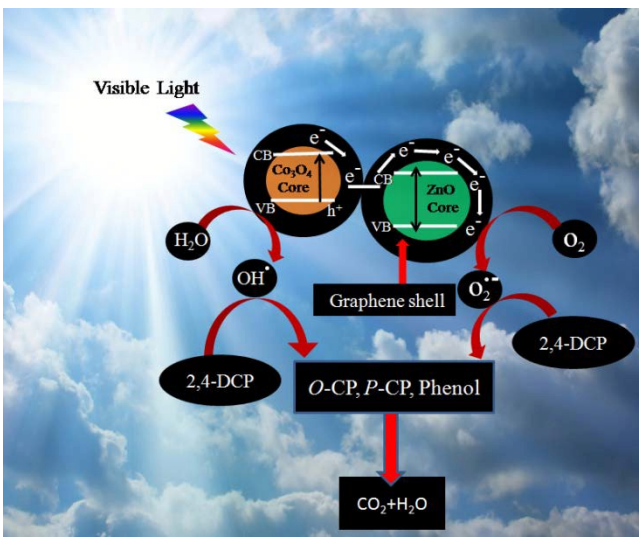

Figure 13. Schematic diagram of photocatalytic mechanism of GE/ZnO/Co_3O_4 core-shell hybrid for the 2,4-DCP degradation under visible light.

A gradual increase in PL intensity at 445 nm is observed with time for GE/ZnO/Co_3O_4 hybrids, which suggests that the fluorescence comes from the chemical reactions between TA and $OH^{\cdot}$ produced during catalytic reactions.[64,65] It is obvious that PL intensity is proportional to the amount of produced hydroxyl radicals. Based on the results, a probable photocatalytic mechanism for the GE/ZnO/Co_3O_4 hybrids is proposed and illustrated in Figure 13. Under visible-light irradiation, electrons (e^-) are excited from the valence band (VB) of Co_3O_4 to its conduction band (CB), leaving the holes in the VB, thereby forming the electron–hole pairs. The photogenerated electrons in the CB can rapidly transfer to the graphene shell due to the intimate interfacial contact between Co_3O_4 and graphene.

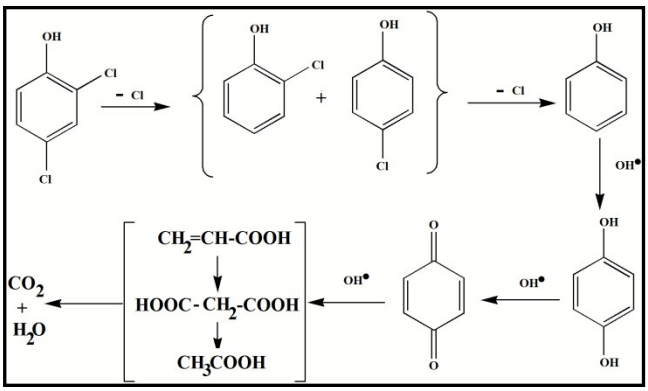

Figure 14. Proposed photodegradation or dechlorination pathways of the 2,4-DCP in presence of the GE/ZnO/Co_3O_4 catalyst under visible light .

As the graphene has excellent electron conductivity, the photogenerated electrons rapidly transfer to the graphene shell of the ZnO resulting significantly enhanced lifetime of photogenerated electron–hole charge carriers. Concurrently, molecular oxygen in the reaction system is activated by reacting

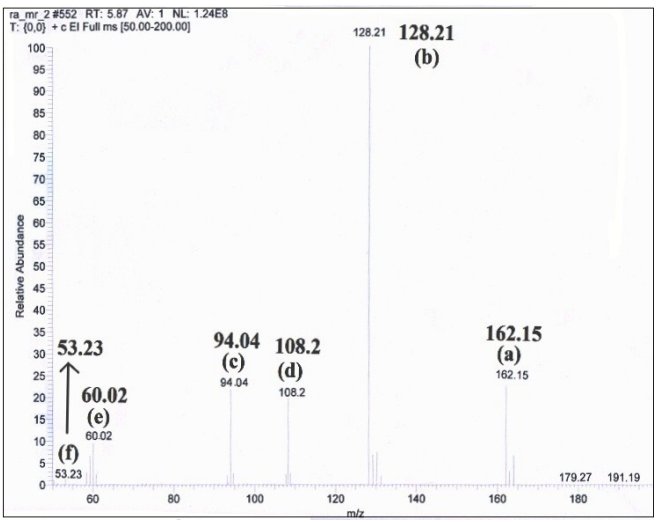

Figure 15. GC-MS spectrum of the photo-degraded products of 2,4-DCP after 2 h of the photocatalytic reaction.

with the photogenerated electrons forming superoxide radicals ($O_2^{\cdot-}$), and the holes of the valence band (VB) of Co_3O_4 react

with water to give hydroxyl radical ($OH^{\cdot}$) as evidenced by the control experiments in Figure 11a. Large amount of $O_2^{\cdot-}$ and $OH^{\cdot}$ are generated in the system due to presence of graphene shell, which act as an effective electron transporter and a continuous electron transfer path is established through the graphene shell on the surface of metal oxide core. The 2,4-DCP adsorbed on the surface of GE/ZnO/Co_3O_4 hybrids, firstly undergoes dechlorination to form *o*-chlorophenol, *p*-chlorophenol and finally phenol, which subsequently reacts with the active species ($OH^{\cdot}$) and converts to para-benzoquinone, which in turn mineralizes into CO_2 and H_2O *via* some intermediates (Figure 14). This also has been confirmed by the GC-MS spectrum (Fig. 15) of the degraded products after 2 h of photocatalytic reaction, which exhibits the peaks of (a) unreacted 2,4-DCP (m/z = 162.15) and its fragmented products, like (b) chlorophenols (m/z = 128.21), (c) phenol (m/z = 94.04), (d) *p*-benzoquinone (m/z = 108.2), (e) acetic acid (m/z = 60.02) and (f) 1,3-butadiene (m/z = 53.23). However, after 5 h of the photoreaction, no peaks related to 2,4-DCP or chlorophenols are observed (Fig. S9) in the GC-MS spectrum indicating maximum mineralization of the 2,4-DCP molecules and also their conversion into fragmented products (of ultra-trace level concentrations) like phenol (m/z = 94.04), *p*-benzoquinone (m/z = 108.2), malonic acid (m/z = 104.01), butenedioic acid (m/z = 116.01), acetic acid (m/z = 60.02) and 1,3-butadiene (m/z = 53.23).

Conclusions

In summary, a novel GE/ZnO/Co_3O_4 core-shell hybrid is successfully fabricated through a facile self-assembly approach driven by mutual electrostatic interaction of the graphene and ZnO/Co_3O_4 heteronanostructure prepared from a thermal decomposition of a nano coordination polymer. The graphene shells enhances the visible light photocatalytic performance of the ZnO/Co_3O_4 core significantly toward degradation and mineralization of aqueous 2,4-DCP. According to different parametric studies, 91% degradation of 2,4-DCP (20 mg/L) is achieved in only 150 min of visible light irradiation in presence of 1.0 g/L of the GE/ZnO/Co_3O_4 catalyst at pH 5.0. The photodegradation of 2,4-DCP follows pseudo-first order kinetics with significantly higher rate constants, 3.3×10^{-2} min^{-1}. It is worth noting that the dechlorination efficiency of the GE/ZnO/Co_3O_4 hybrid is significantly higher than some previous reports. Moreover, the GE/ZnO/Co_3O_4 core-shell hybrid possesses high stability in comparison with normal graphene based hybrids, and has been successfully recycled up to five cycles without any significant loss of photocatalytic activity. The improvement in photocatalytic activity and stability of GE/ZnO/Co_3O_4 core-shell hybrid can be ascribed by an increase in contact surface between metal oxide core and graphene shell more effectively than the traditional graphene-metal oxide composites. We presume that the association of graphene contact serves as a continuous path for rapid shuttle of electrons producing more reactive species (superoxide and hydroxyl). On the other hand, it also helps preventing the aggregation and photocorrosion of ZnO/Co_3O_4 core in a more effective way. Overwhelmingly, the higher rate of mineralization (93% in 5 h) offered by the GE/ZnO/Co_3O_4 hybrid would make it a potential candidate for visible light photocatalytic degradation or dechlorination of chlorinated phenols, wastewater treatment as well as in different energy conversion systems.

Acknowledgements

The author, MR, thanks the CSIR for research fellowship. Further, the authors extend their acknowledgments to CRF-IITKGP for TEM, HRTEM, EDX analysis. The authors also acknowledge the SERB, New Delhi for financial support (Project code: SDP & Ref. No.: SR/FT/CS-146/2011) and DST-FIST for XPS facility (Department of Physics, IIT Kharagpur).

Author Information

*Corresponding author: +91-3222-282322; e-mail: raja@chem.iitkgp.ernet.in

References

1. J. Zhang, J. G. Yu, M. Jaroniec and J. R. Gong, Noble Metal-free Reduced Graphene Oxide-$Zn_xCd_{1-x}S$ Nanocomposite with Enhanced Solar Photocatalytic H_2 Production Performance, *Nano Lett.*, 2012, **12**, 4584−4589.
2. Q. J. Xiang, J. G. Yu and M. Jaroniec, Graphene-Based Semiconductor Photocatalyst, *Chem. Soc. Rev.*, 2012, **41**, 782−796.
3. P. V. Kamat, Graphene-Based Nanoassemblies for Energy Conversion, *J. Phys. Chem. Lett*., 2011, **2**, 242−251.
4. T. Xu, L. Zhang, H. Cheng and Y. Zhu, Significantly Enhanced Photocatalytic Performance of ZnO via Grapheme Hybridization and the Mechanism Study, *Appl. Catal. B: Environ*., 2011, **101**, 382-387.
5. A. K. Geim, Graphene: Status and Prospects, *Science*, 2009, **324**, 1530−1534.
6. S. Stankovich, D. A. Dikin, G. H. B. Dommett, K. M. Kohlhaas, E. J. Zimney, E. A. Stach, , R. D. Piner, S. T. Nguyen and R. S. Ruoff, Graphene-Based Composite Materials, *Nature*, 2006, **442**, 282−286.
7. H. Zhang, X. J. Lv, Y. M. Li, Y. Wang and J. H. Li, P25-Graphene Composite as a High Performance Photocatalyst, *ACS Nano*, 2010, **4**, 380−386.
8. Y. Zhang, Z. R. Tang, X. Fu and Y. J. Xu, TiO_2−Graphene Nanocomposites for Gas-Phase Photocatalytic Degradation of Volatile Aromatic Pollutant: Is TiO_2−Graphene Truly Different from Other TiO_2−Carbon Composite Materials? *ACS Nano*, 2010, **4**, 7303−7314.
9. X. Huang, X. Y. Qi, , F. Boey and H. Zhang, Graphene-Based Composites, *Chem. Soc. Rev*., 2012, **41**, 666−686.
10. Y. Bu, Z. Chen, W. Li and B. Hou, Highly Efficient Photocatalytic Performance of Graphene–ZnO Quasi-Shell–Core Composite Material, *ACS Appl. Mater. Interfaces*, 2013, **5**, 12361−12368.
11. L. Hu, P. Zhang, Y. Sun, S. Bao and Q. Chen, ZnO/Co_3O_4 Porous Nanocomposites Derived from MOFs: Room-Temperature Ferromagnetism and High Catalytic Oxidation of CO, *ChemPhysChem*, 2013, **14**, 3953 – 3959.
12. A. Brinkman, M. Huijben, M. V. Zalk, , J. Huijben, U. Zeitler, J. C. Maan, W. G. V. Wiel, G. Rijnders, D. H. A. Blank and H. Hilgenkamp, Magnetic Effects at the Interface Between Non-Magnetic Oxides, *Nat. Mater.*, 2007, **6**, 493 –496.
13. F. Y. Bruno, J. G. Barriocal, M. Torija, A. Rivera, Z. Sefrioui, C. Leighton, C. Leon and J. Santamaria, Effects of Interface States on the Transport Properties of All-oxide La 0.8 Sr 0.2 CoO 3/SrTi 0.99 Nb 0.01 O 3 pn Heterojunctions, *Appl. Phys. Lett*., 2008, **92**, 082106-082109.
14. J. S. Chen, C.P. Chen, J. Liu, R. Xu, S. Z. Qiao, and X. W. Lou, Ellipsoidal Hollow Nanostructures Assembled from Anatase TiO_2 Nanosheets as a Magnetically Separable Photocatalyst. *Chem. Commun.*, 2011, **47**, 2631 –2633.
15. X. W. Liu, Z. Fang, X. J. Zhang, W. Zhang, X. W. Wei and B. Y. Geng, Preparation and Characterization of Fe_3O_4/CdS

Nanocomposites and Their Use as Recyclable Photocatalysts, *Cryst. Growth Des*, 2009, **9**, 197– 202.
16. Y. Hu, H. H. Qian, Y. Liu, G. H. Du, F. M. Zhang, L. B. Wang and X. Hu, A Microwave-Assisted Rapid Route to Synthesize ZnO/ZnS Core–Shell Nanostructures via Controllable Surface Sulfidation of ZnO Nanorods, *CrystEngComm*, 2011, **13**, 3438 –3443.
17. D. Bekermann, A. Gasparotto, D. Barreca, C. Maccato, E. Comini, C. Sada, G. Sberveglieri, A. Devi and R. A. Fischer, Co_3O_4/ZnO Nanocomposites: From Plasma Synthesis to Gas Sensing Applications, *ACS Appl. Mater. Interfaces*, 2012, **4**, 928– 934.
18. X. W. Xie, Y. Li, Z. Q. Liu, M. Haruta and W. J. Shen, Low-Temperature Oxidation of CO Catalysed by Co_3O_4 Nanorods, *Nature*, 2009, **458,** 746 – 749.
19. X. L. Xiao, X. F. Liu, H. Zhao, D. F. Chen, F. Z. Liu, J. H. Xiang, Z. B. Hu and Y. D. Li, Facile Shape Control of Co_3O_4 and the Effect of the Crystal Plane on Electrochemical Performance, *Adv. Mater.*, 2012, **24**, 5762 –5766.
20. C. W. Na, H. S. Woo, I. D. Kim and J. H. Lee, Selective Detection of NO_2 and C_2H_5OH Using a Co_3O_4-Decorated ZnO Nanowire Network Sensor, *Chem. Commun.*, 2011, **47**, 5148 – 5150.
21. C. Zhu, S. Guo, P. Wang, L. Xing, Y. Fang, Y. Zhai and S. Dong, One-Pot Water-Phase Approach to High-Quality Graphene/TiO_2 Composite Nanosheets, *Chem. Commun*., 2010, **46**, 7148−7150.
22. R. C. Pawar and C. S. Lee, Single-Step Sensitization of Reduced Graphene Oxide Sheets and CdS Nanoparticles on ZnO Nanorods as Visible-Light Photocatalysts, *Appl. Catal. B*: *Environ*, 2014, **144**, 57–65.
23. J. Yu, J. Zhang and M. Jaroniec, Preparation and Enhanced Visible-Light Photocatalytic H_2-Production Activity of CdS Quantum Dots-Sensitized $Zn_{1-x}Cd_xS$ Solid Solution, *Green Chem.*, 2010, **12**, 1611−1614.
24. S. Zhuang, X. Xu, B. Feng, J. Hu, Y. Pang, G. Zhou, L. Tong and Y. Zhou, Photogenerated Carriers Transfer in Dye–Graphene–SnO_2 Composites for Highly Efficient Visible-Light Photocatalysis, *ACS Appl. Mater. Interfaces*, 2014, **6**, 613−621.
25. S. Yang, X. Feng, S. Ivanovici and K. Mullen, Porous Iron Oxide Ribbons Grown on Graphene for High-Performance Lithium Storage, *Angew. Chem. Int. Ed*., 2010, **49**, 8408 –8410.
26. M. Rakibuddin and R. Ananthakrishnan, Porous ZnO/Co_3O_4 Heteronanostructures Derived from Nano Coordination Polymers for Enhanced Gas Sorption and Visible Light Photocatalytic Applications, *RSC Adv*., 2015, **5**, 68117-68127.
27. W. S. Hummers and R. E. Offeman, Preparation of Graphitic Oxide, *J. Am. Chem. Soc.*, 1958, **80**, 1339-1339.
28. C. Nethravathi and M. Rajamathi, Chemically Modified Graphene Sheets Produced by the Solvothermal Reduction of Colloidal Dispersions of Graphite Oxide, *Carbon*, 2008, **46**, 1994-1998.
29. J. Zhang, Z. Xiong and X. S. Zhao, Graphene–Metal–Oxide Composites for the Degradation of Dyes under Visible Light Irradiation, *J. Mater. Chem*., 2011, **21**, 3634-3640.
30. H. Nguyen and S. A. El-Safty, Meso- and Macroporous Co_3O_4 Nanorods for Effective VOC Gas Sensors, *J. Phys. Chem. C*, 2011, **115**, 8466–8474.
31. Z. Alizadeh, K.B. Sundaram and S. Seal, The Effect of Nitrogen on the Chemistry of Sputter-Deposited SiC_xN_y Films, *Appl. Surf. Sci.*, 2001, **183**, 270-277.
32. I. E. Bordianu, G. David, B. Simionescu, M. Aflori, C. Ursu, A. Coroaba, G. Hitruc, C. Cotofana and M. Olaru, Functional Silsesquioxane-Based Hierarchical Assemblies for Antibacterial/Antifungal Coatings, *J. Mater. Chem. B*, 2015, **3**, 723-727.
33. C. Yuan, J. Li, L. Hou, L. Yang, L. Shen and X. Zhang, Facile Template-Free Synthesis of Ultralayered Mesoporous Nickel Cobaltite Nanowires Towards High-Performance Electrochemical Capacitors, *J. Mater. Chem*., 2012, **22**, 16084-16090.
34. L. Guo, Y. L. Ji, H. Xu, P. Simon and Z. Wu, Regularly Shaped, Single-Crystalline ZnO Nanorods with Wurtzite Structure, *J. Am. Chem. Soc*., 2002, **124**, 14864 – 14865.
35. X.W. Lou, C. M. Li and L. A. Archer, Designed Synthesis of Coaxial SnO_2@carbon Hollow Nanospheres for Highly Reversible Lithium Storage, *Adv. Mater*., 2009, **21**, 2536-2539.
36. Y. S. Hu, R. D. Cakan, M. M. Titirici, J. O. Muller, R. Schlogl, M. Antonietti and J. Maier, Superior Storage Performance of a Si@SiO_x/C Nanocomposite as Anode Material for Lithium-ion Batteries., *Angew. Chem.Int. Ed.*, 2008, **120**, 1669-1673.
37. W. M. Zhang, J. S. Hu, Y. G. Guo, S. F. Zheng, L. S. Zhong, W. G. Song and L. J. Wan, Tin-Nanoparticles Encapsulated in Elastic Hollow Carbon Spheres for High-Performance Anode Material in Lithium-Ion Batteries, *Adv. Mater.*, 2008, **20**, 1160-1165.
38. S. Some, Y. Kim, E. Hwang, H. Yoo and H. Lee, Binol Salt as a Completely Removable Graphene Surfactant, *Chem. Commun*., 2012, **48**, 7732–7734.
39. Y. Chen, K. Munechika and D. S. Ginger, Dependence of Fluorescence Intensity on the Spectral Overlap between Fluorophores and Plasmon Resonant Single Silver Nanoparticles, *Nano Lett*., 2007, **7**, 690-696.
40. I. Alemzadeh and S. Nejati, Phenols Removal by Immobilized Horseradish Peroxidase, *J. Hazard. Mater*., 2009, **166**, 1082–1086.
41. H. Wang and J. Wang, Electrochemical Degradation of 4-Chlorophenol Using a Novel Pd/C Gas-Diffusion Electrode, *Appl. Catal. B*: *Environ*., 2007, **77**, 58–65.
42. J. B. Jia, S. P. Zhang, P. Wang and H. J. Wang, Degradation of High Concentration 2,4-Dichlorophenol by Simultaneous Photocatalytic–Enzymatic Process Using TiO2/UV and Laccase, *J. Hazard. Mater*., 2012, **205**, 150–155.
43. M. Rakibuddin and R. Ananthakrishnan, Iron(II) phenanthroline-resin hybrid as a visible light-driven heterogeneous catalyst for green oxidative degradation of organic dye, *Catal. Commun*., 2015, **58**, 53–58.
44. R. Ananthakrishnan and S. Gazi, $[Ru(bpy)_3]^{2+}$ aided photocatalytic synthesis of 2-arylpyridines via Hantzsch reaction under visible irradiation and oxygen atmosphere, *Catal. Sci. Technol*., 2012, **2**, 1463–1471.
45. S. Gazi and R. Ananthakrishnan, Metal-free-photocatalytic reduction of 4-nitrophenol by resin-supported dye under the visible irradiation, *Appl. Catal. B: Environ*, 2011, **105**, 317–325.
46. S. Gazi and R. Ananthakrishnan, Bromodimethylsulfonium bromide as a potential candidate for photocatalytic selective oxidation of benzylic alcohols using oxygen and visible light, *RSC Adv.*, 2012, **2**, 7781-7787.
47. S. Bhar and R. Ananthakrishnan, Utilization of Ru(II)-complex immobilized ZnO hybrid in presence of Pt(II) co-catalyst for photocatalytic reduction of 4-nitrophenol under visible light, *RSC Adv.*, 2015, **5**, 20704.
48. P. Wu, C. Liu, Z. Huang, W. Wang, Enhanced Dechlorination Performance of 2,4-Dichlorophenol by Vermiculite Supported Iron Nanoparticles Doped with Palladium, *RSC Adv*., 2014, **4**, 25580-25587.
49. G. Liao, S. Chen, X. Quan, Y. Hongtao and H. Zhao, Graphene Oxide Modified g-C_3N_4 Hybrid with Enhanced Photocatalytic Capability under Visible Light Irradiation, *J. Mater. Chem*., 2012, **22**, 2721–2726.
50. S. Li, X. Ma, L. Liu and X. Cao, Degradation of 2,4-Dichlorophenol in Wastewater by Low Temperature Plasma Coupled with TiO_2 Photocatalysis, *RSC Adv*., 2015, **5**, 1902-1909.
51. D. Zhao, Y. Zheng, M. Li, S. Ali Baig, D. Wu and X. Xu, Catalytic dechlorination of 2,4-dichlorophenol by Ni/Fe nanoparticles prepared in the presence of ultrasonic irradiation, *Ultrason. Sonochem*., 2014 **21**, 1714–1721.
52. L. Yin, Z. Shen, J. Niu, J. Chen and Y. Duan, Degradation of Pentachlorophenol and 2,4-Dichlorophenol by Sequential Visible-Light Driven Photocatalysis and Laccase Catalysis, *Environ. Sci. Technol.*, 2010, **44**, 9117–9122.
53. P. Chowdhury, J. Moreira, H. Gomaa and A. K. Ray, Visible-Solar-Light-Driven Photocatalytic Degradation of Phenol with Dye-Sensitized TiO2: Parametric and Kinetic Study, *Ind. Eng. Chem. Res.*, 2012, **51**, 4523-4532.
54. D. Chen and A. K. Ray, Photodegradation kinetics of 4-nitrophenol in TiO_2 suspension, *Water. Res.*, 1998, **32**, 3223-3234.
55. S. K. Pardeshi and A. B. Patil, A Simple Route for Photocatalytic Degradation of Phenol in Aqueous Zinc Oxide Suspension Using Solar Energy, *Sol. Energy*, 2008, **82**, 700-705.

56. S. Sakthivel, B. Neppolian, M. V. Shankar, B. Arabindoo, M. Palanichamy and V. Murugesan, Solar Photocatalytic Degradation of Azo Dye: Comparison of Photocatalytic Efficiency of ZnO and TiO_2, *Sol. Energy Mater. Sol. Cells*, 2003, **77**, 65-82.
57. S. Ardizzone, G. Spinolo and S. Trasatti, The Point of Zero Charge of Co_3O_4 Prepared by Thermal Decomposition of Basic Cobalt Carbonate, *Electrochim. Acta*, 1995, **40**, 2683-2686.
58. H. Li, Z. Xia, J. Chen, L. Lei and J. Xing, Constructing Ternary CdS/Reduced Graphene Oxide/TiO_2 Nanotube Arrays Hybrids for Enhanced Visible-Light-Driven Photoelectrochemical and Photocatalytic Activity, *Appl. Catal. B: Environ*, 2015, **168**, 105–113.
59. X. Yang, J. Qin, Y. Jiang, K. Chen, X. Yan, D. Zhang, R. Li and H. Tang, Fabrication of P25/Ag_3PO_4/Graphene Oxide Heterostructures for Enhanced Solar Photocatalytic Degradation of Organic Pollutants and Bacteria, *Appl. Catal. B: Environ*, 2015, **166**, 231–240.
60. S. Zhuang, X. Xu, B. Feng, J. Hu, Y. Pang, G. Zhou, L. Tong and Y. Zhou, Photogenerated Carriers Transfer in Dye–Graphene–SnO_2 Composites for Highly Efficient Visible-Light Photocatalysis, *ACS Appl. Mater. Interfaces*, 2014, **6**, 613−621.
61. M. Stylidi, D. I. Kondarides and X. E. Verykios, Visible Light-Induced Photocatalytic Degradation of Acid Orange 7 in Aqueous TiO_2 Suspensions, *Appl. Catal. B*: *Environ*, 2004, **47**, 189–201.
62. N. Zhang, Y. Zhang, M. Q. Yang, Z. R. Tang and Y. J. Xu, A Critical and Benchmark Comparison on Graphene, Carbon Nanotube, and Fullerene-Semiconductor Nanocomposites as Visible Light Photocatalysts for Selective Oxidation, *J. Catal.* 2013, **299**, 210–221.
63. Y. Jiang and T. P. Loh, Catalytic and Direct Methyl Sulfonylation of Alkenes and Alkynes Using a Methyl Sulfonyl Radical Generated from a DMSO, Dioxygen and Copper System, *Chem. Sci.*, 2014, **5**, 4939-4943.
64. J. Yu, W. Wang, B. Cheng and B. L. Su, Enhancement of Photocatalytic Activity of Mesporous TiO_2 Powders by Hydrothermal Surface Fluorination Treatment, *J. Phys. Chem. C*, 2009, **113**, 6743–6750.
65. T. Rhadfi, J. Y. Piquemal, L. Sicard, F. Herbst, E. Briot, M. Benedetti and A. Atlamsani, Polyol-Made Mn_3O_4 Nanocrystals as Efficient Fenton-Like Catalysts, *Appl. Catal., A: Gen.*, 2010, **386**, 132–139.

Graphical Abstract

Effective Photocatalytic Dechlorination of 2,4-Dichlorophenol by A Novel Graphene Encapsulated ZnO/Co_3O_4 Core-shell Hybrid under Visible Light

Md.Rakibuddin and Rajakumar Ananthakrishnan*

Department of Chemistry, Indian Institute of Technology, Kharagpur 721 302, India.